

## Observations of low-frequency magnetic oscillations in the Martian magnetosheath, magnetic pileup region, and tail

J. R. Espley,<sup>1</sup> P. A. Cloutier,<sup>1</sup> D. A. Brain,<sup>2</sup> D. H. Crider,<sup>3</sup> and M. H. Acuña<sup>4</sup>

Received 14 August 2003; revised 11 April 2004; accepted 13 May 2004; published 31 July 2004.

[1] Observations are presented of low-frequency magnetic oscillations in the Martian magnetosheath, magnetic pileup region, and tail as observed by the Magnetometer/Electron Reflectometer experiment on board Mars Global Surveyor. Within the dayside magnetosheath the oscillations are found to be predominantly compressional, elliptically polarized waves with wave vectors that have large angles relative to the mean field and dominant frequencies that are significantly below the local proton gyrofrequency. On the basis of these observations we identify these oscillations as mirror mode instabilities. In the nightside magnetosheath the oscillations are predominantly transverse and elliptical, and they propagate at smaller angles relative to the mean field at frequencies within a factor of 2–10 less than the local proton gyrofrequency. These characteristics lead us to associate these oscillations with ion/ion-resonant instabilities that arise from counterstreaming plasma populations such as the solar wind and pickup ions of planetary origin. Within the magnetic pileup region and tail the oscillations have considerably smaller amplitudes and are linearly polarized, obliquely propagating, ultralow-frequency oscillations which may be a mix of multiple wave modes. *INDEX TERMS*: 5443 Planetology: Solid Surface Planets: Magnetospheres (2756); 6025 Planetology: Comets and Small Bodies: Interactions with solar wind plasma and fields; 6225 Planetology: Solar System Objects: Mars; 7871 Space Plasma Physics: Waves and instabilities; 7867 Space Plasma Physics: Wave/particle interactions; *KEYWORDS*: Mars, magnetic oscillations, magnetosheath, solar interaction, low frequency

**Citation:** Espley, J. R., P. A. Cloutier, D. A. Brain, D. H. Crider, and M. H. Acuña (2004), Observations of low-frequency magnetic oscillations in the Martian magnetosheath, magnetic pileup region, and tail, *J. Geophys. Res.*, 109, A07213, doi:10.1029/2003JA010193.

### 1. Introduction

[2] Mars lacks a global intrinsic magnetic field [Acuña *et al.*, 1998], so its interaction with the solar wind is similar to the Venusian [Cloutier *et al.*, 1999] and cometary [Mazelle *et al.*, 1995] interactions. Such interactions produce a variety of plasma boundaries and disturbances. The main boundary is a bow shock where the supersonic solar wind is slowed as it is diverted around the obstacle created by the ionosphere. Additional boundaries are commonly produced downstream of the shock. In the case of Mars one such boundary is the magnetic pileup boundary (MPB), which was identified by Vignes *et al.* [2000] using data from the Mars Global Surveyor (MGS) Magnetometer/Electron Reflectometer

(MAG/ER) investigation [Acuña *et al.*, 1998]. This boundary is the same boundary as the planetopause reported by Trotignon *et al.* [1996] using Phobos 2 data. Similar boundaries have been identified at comets [Neubauer *et al.*, 1986] and at Venus [Bertucci *et al.*, 2003a].

[3] In addition to plasma boundaries, magnetic and plasma disturbances are important and common features created by solar wind interactions. Such phenomena are interesting because in a collisionless plasma these fluctuations act as a key method of redistributing energy in the system. Additionally, at Mars they are related to pickup ion processes and are therefore important to studies of atmospheric loss and climate change [Jakosky and Phillips, 2001]. Furthermore, studying these fluctuations is important in order to understand the energetic particle environment at both the surface and in space (“space weather”) and to understand the origin of low-frequency electromagnetic signals detectable at the surface.

[4] Studies of low-frequency plasma waves have been done for most objects in the solar system, though with unequal degrees of completeness. Huba and Strangeway [1997] summarize in a review article much of the current understanding of plasma waves at Venus. Plasma waves have been found across many frequency ranges, and the observations include waves observed both upstream of the

<sup>1</sup>Department of Physics and Astronomy, Rice University, Houston, Texas, USA.

<sup>2</sup>Space Sciences Laboratory, University of California, Berkeley, California, USA.

<sup>3</sup>Department of Physics, Catholic University of America, Washington, D. C., USA.

<sup>4</sup>NASA Goddard Space Flight Center, Greenbelt, Maryland, USA.

bow shock and in the regions between the bow shock and the ionosphere. At the low-frequency (LF) range (used here to refer to frequencies near or below the proton gyrofrequency) and at the ultralow-frequency (ULF) range (below the lowest common ion gyrofrequency of the plasma), however, comparatively little work has been done, especially downstream of the bow shock. *Strangeway and Crawford* [1995] and *Orlowski et al.* [1990] identified some ULF oscillations in the region upstream of the Venusian bow shock, and *Orlowski et al.* [1994] were able to compare such oscillations to specific wave modes predicted by linear Vlasov theory and Hall-MHD theory. *Brace et al.* [1983] were able to identify ULF waves in the nightside ionosphere of Venus. *Luhmann et al.* [1983] determined that ULF fluctuations in the Venusian magnetosheath could be associated with fluctuations at the shock that are convected into the magnetosheath. *Winske* [1986] offered an alternative explanation associating the fluctuations with beam instabilities created by the interaction of the solar wind with newly born ions of planetary origin. *Luhmann et al.* [1987] examined the role of plasma fluctuations and quasi-parallel shocks on pickup ion escape. Recent work by *Grebowsky et al.* [2003] identifies ULF waves associated with pickup ions in the Venusian ionosheath.

[5] LF waves at comets have received more study. Several review papers lay out the basic theory and observations of LF and ULF waves at comets [*Lee*, 1989; *Ip and Axford*, 1990; *Tsurutani*, 1991a, 1991b]. Several papers report observations made of ULF waves both upstream of cometary bow shocks and downstream in the cometary magnetosheaths and the magnetic pileup regions [*Tsurutani and Smith*, 1986a, 1986b; *Glassmeier et al.*, 1987; *Mazelle et al.*, 1991; *Glassmeier and Neubauer*, 1993; *Glassmeier et al.*, 1993; *Neubauer et al.*, 1993].

[6] Studies of LF and ULF waves in the Earth's magnetosheath have been conducted for decades (see reviews by *Gary et al.* [1993], *Hubert* [1994], *Omidi et al.* [1994], *Lacombe and Belmont* [1995], and *Schwartz et al.* [1996]). Such studies provide the basis for understanding similar phenomena elsewhere in the solar system.

[7] At Mars, detailed observations of plasma waves started with Phobos 2 [*Riedler et al.*, 1989; *Grard et al.*, 1989; *Sagdeev et al.*, 1990]. ULF waves near the proton gyrofrequency have been observed upstream of the Martian bow shock using both Phobos 2 data [*Russell et al.*, 1990, 1992; *Tarasov et al.*, 1998; *Delva and Dubinin*, 1998] and MGS data [*Brain et al.*, 2002]. Initial reports of ULF waves within the magnetosheath and the magnetic pileup region as observed by MGS have also been made [*Cloutier et al.*, 1999; *Crider*, 1999; *Bertucci et al.*, 2003b; *Grebowsky et al.*, 2003]. In this work, we present detailed studies of LF waves within the Martian magnetosheath (the region between the bow shock and MPB), magnetic pileup region (MPR), and the tail. Generally, the MPR is defined as the region between the MPB and the photoelectron boundary discovered by MGS [*Mitchell et al.*, 2000]. In this paper, we use the term to refer to any locations below the MPB. We report on the amplitudes, polarization, and frequencies of magnetic oscillations

sampled by MGS during its premapping mission phases and discuss the wave modes implied by the observations.

## 2. MGS Data Set

[8] The MAG/ER investigation on MGS has been returning data on the Martian plasma environment since its arrival at Mars in September 1997. More detailed descriptions of the MAG/ER instrument and data set are available elsewhere [*Acuña et al.*, 2001]. Here we present only information necessary to understand the data used in this investigation. Two redundant triaxial vector magnetometers provide measurements of the ambient magnetic field with a maximum data rate of 32 samples per second with a range of  $\pm 4$  to  $\pm 65,536$  nT. The spacecraft passed through several mission phases before reaching its mapping orbit. These "premapping" orbits are particularly useful for investigations of the Martian plasma environment since their evolving orbital characteristics allowed the spacecraft to sample many locations of interest, including the bow shock, the magnetosheath, and the magnetic pileup region. The magnetometer (MAG) data used in this work include data from most of the orbits of the aerobraking phases and from the science phasing orbits [*Albee et al.*, 2001].

[9] The MAG data rate varied between 32, 16, and 8 samples per second according to the telemetry requirements of the spacecraft. Every 24th datum was recorded at its full value ("full word"), and all samples in between recorded only the difference from the last full value. This created both high (using all available samples) and low (using only the full word samples) time resolution data. Since the magnetometers were located on the solar panels, currents from some of the electronics on board the spacecraft produced fields that were detected by the instruments. However, using a spacecraft magnetic field model developed from calibration maneuvers, this static and dynamic background has been largely removed from the low time resolution data [*Acuña et al.*, 2001]. For the high time resolution data the dynamic background could not be subtracted because the engineering data used to calibrate the full word measurements could not be reliably interpolated to create dynamically calibrated high time resolution data. This dynamic spacecraft field is expected to vary with the spacecraft spin period of  $\sim 100$  min. Furthermore, even the low time resolution data are estimated to be only reliably calibrated to within  $\pm 3$  nT. The calibration is expected to be considerably better ( $< 0.5$  nT) for measurements made on the nightside (J. E. P. Connerney, personal communication, 2003).

[10] For these reasons we use the low time resolution data to calculate the magnitude of the magnetic field, which we then use to calculate quantities such as the ion gyrofrequencies. We use the high time resolution data to calculate quantities that are relative to the mean magnetic field and for spectral analysis. Thus we use the most fully calibrated data when necessary and use the highest time resolution data when possible.

[11] The MAG data used here are given in the Sun state (SS) Cartesian coordinate system. In this system the Mars-Sun line is defined as the  $+x$  direction, the orbital motion of Mars is the  $-y$  direction, and the  $+z$  axis completes the orthogonal set (and is roughly northward on Mars). This

coordinate system is one of the systems used by the instrument team in its production of the data [Acuña *et al.*, 2001], is comparable to the geocentric solar ecliptic and the Venus solar orbital coordinate systems, and is the same as the Mars solar orbital system.

### 3. Data Analysis

[12] In this section we present our results of analyses done on the polarizations, amplitudes, directions of propagation, and frequencies of the magnetic oscillations. For many of these analyses we use a mean field (MF) coordinate system. In our MF coordinate system the principal direction is defined as the direction of the mean magnetic field over some given time interval, the second direction is perpendicular to the mean field and contains no  $z$  component from the SS measurements, and the third direction is perpendicular to the other two directions. Perturbations from this mean field can then be calculated in each of these directions for every measurement within the time interval. The interval chosen is long enough so that several cycles of the principal characteristic frequencies (the proton and oxygen gyrofrequencies) are included but short enough so that the mean field itself does not vary significantly during that interval. This means that for most analyses we used 60 sec intervals. This implies that we are effectively band-pass filtering our data so that oscillations with periods greater than 60 sec do not contribute significantly to our statistical results. For this work we accept such limitations since they allow us to avoid “signals” created by the spacecraft simply sampling different plasma regions over long periods of time. We hope to, in future work, examine longer period signals by using specific orbits.

[13] Minimum variance analysis (MVA) is another analysis tool we use. Minimum variance analysis works by finding the direction of the minimum variance of the mean magnetic field. Mathematically, this direction is found by solving for the eigenvector associated with the minimum eigenvalue of the covariance or spectral matrix [Sonnerup and Cahill, 1967; Means, 1972; McPherron *et al.*, 1972; Arthur *et al.*, 1976; Song and Russell, 1999]. This direction is then assumed to be the direction of propagation of the wave (or in the case of stationary structures to be the direction of the wave vector), and the ellipticity and polarization of the variations can also be calculated. This method assumes planarity of the waves and also assumes that one major wave mode dominates such that the wave vector direction determined is of that mode. This method also does not work well for waves with nearly linear polarization since the minimum and intermediate eigenvalues are very similar in such a case. For all these reasons, results from MVA should be treated cautiously, especially in regions of nearly linear polarization (see Figure 1), although the method remains important for obtaining first-order results about the directions of the wave vectors.

[14] Another important point is that we generally used data from nearly all premapping orbits (a few orbits had data irregularities that made their use difficult), which means that many of the statistical results that we present for low altitudes are affected by the crustal magnetic sources. However, although detectable up to at least 1000 km in altitude [Brain, 2002], the strongest sources

cover a relatively small fraction of the Martian surface. It is expected therefore that their effect on statistical results will be small. Nevertheless, we hope in future work to perform detailed analyses of the MPR, including analysis of data from orbits that are free from the effects of the crustal magnetic sources.

#### 3.1. Statistical Results

[15] We present first statistical analyses done for all usable premapping orbits and then present selected orbits as case studies.

##### 3.1.1. Ellipticity

[16] We consider first the ellipticity of the oscillations about the mean field for a particular interval using minimum variance analysis. Starting with the data in MF coordinates for a given 60 sec interval, we use the conventional definition of ellipticity,

$$\epsilon = \sqrt{\frac{b^2}{a^2}}, \quad (1)$$

where  $a$  and  $b$  are the semimajor and semiminor axes, respectively, of the best fit ellipse created by the oscillations about the mean field. In this convention,  $\epsilon$  of 1 implies a perfect circle, whereas  $\epsilon$  of 0 implies a straight line.

[17] Figure 1 shows our results for the 484 orbits that contained usable data. The color scale shows the ellipticity for a given interval in SS coordinates. An outline of Mars and the best fit locations of the bow shock and MPB [Vignes *et al.*, 2000] are shown. Each pixel of the map has height and width of 1/10th of the Martian radius. Several features are immediately obvious. The oscillations are only moderately elliptically polarized in the dayside magnetosheath relative to the fairly circular ellipticity observed in the upstream oscillations. The oscillations in the nightside magnetosheath (solar zenith angles greater than  $90^\circ$ ) are more varied and are sometimes fairly circular. The oscillations in the MPR and in the tail region are generally quite linearly polarized.

##### 3.1.2. Polarization

[18] Figure 2 shows a similar map in SS coordinates for the sense of polarization of the oscillations. Using the MF coordinate system, we determine the relative average sense of rotation about the mean field for a given time interval. Regions that had, on average, intervals that were predominantly left-hand polarized are shown with bluer colors, whereas regions that had, on average, right-hand polarization are shown with redder colors. As can be seen, the results are fairly mixed, but a few trends are apparent. Generally, in the nightside magnetosheath the waves are left-hand polarized, as are some regions in the dayside magnetosheath. It is important to note that these senses of polarization are observed in the spacecraft frame and also that for regions that are predominantly linearly polarized (such as the MPR and tail), discussions of senses of polarization are largely irrelevant.

##### 3.1.3. Mean Field Amplitudes

[19] Figure 3 shows a map in SS coordinates of the difference between the relative amplitudes of the oscillations perpendicular and parallel to the mean field for a given 60 sec interval. The measurements were produced by rotating into the MF coordinate system from SS coordinates

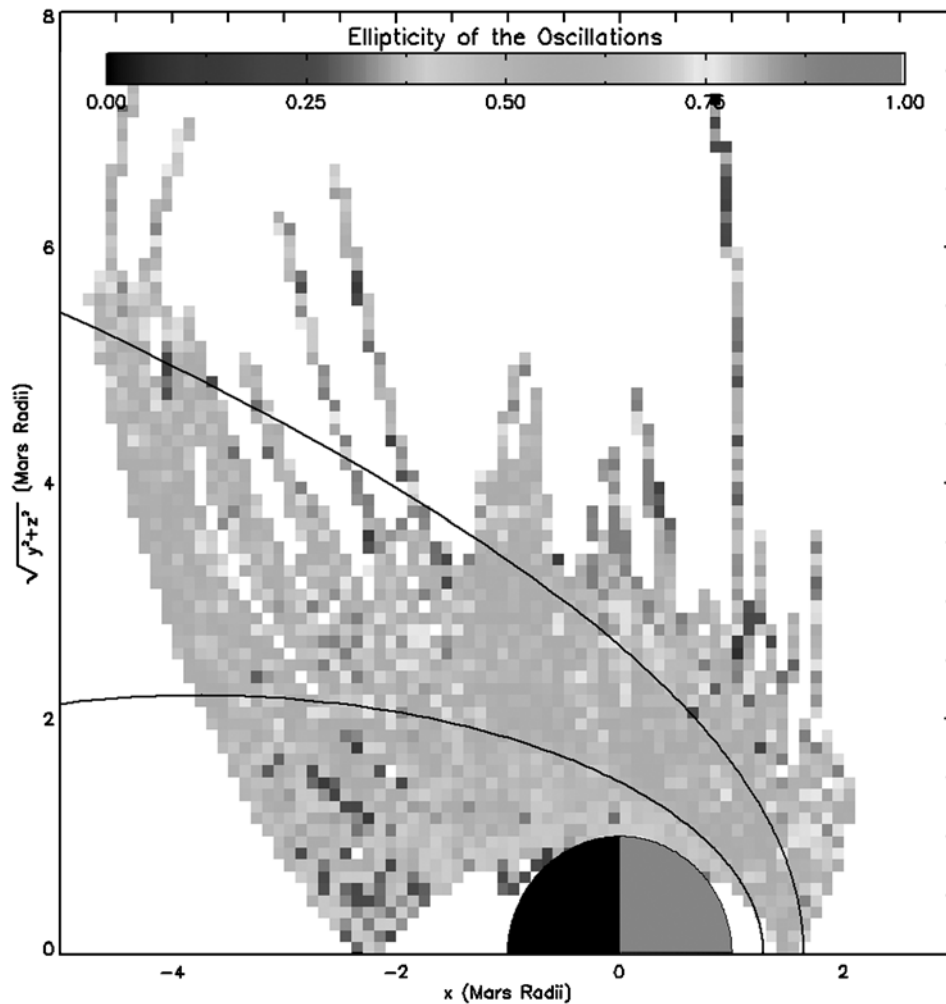


**Figure 1.** Map in Sun state (SS) coordinates of the ellipticity of the oscillations relative to the mean field. See color version of this figure at back of this issue.

and then finding the average amplitudes in the perpendicular ( $\langle \delta B_{\perp} \rangle$ ) and parallel ( $\langle \delta B_{\parallel} \rangle$ ) directions. The difference is normalized by  $|B|$ .

[20] Within the dayside magnetosheath the parallel oscillations are larger, and thus the waves are largely compressional. In the nightside magnetosheath the results are more mixed, but the oscillations tend to be more perpendicular, and thus the waves there are transverse. In the MPR and tail the oscillations are neither preferentially compressional nor preferentially transverse.

#### 3.1.4. Wave Vector Directions

[21] Figure 4 shows a map of the likely directions of propagation of the dominant wave mode relative to the mean field ( $\Theta_{\mathbf{k}, \mathbf{B}}$ ). In the case of standing modes the direction determined is that of the wave vector. We show only measurements that have intermediate to minimum eigenvalue ratios greater than 2 [Song and Russell, 1999]. The results show that in the dayside magnetosheath, MPR, and tail the dominant wave modes have wave vectors at angles between  $65^{\circ}$  and  $90^{\circ}$ , that is, fairly perpendicular relative to the mean magnetic field. From the terminator extending into the nightside magnetosheath, the waves have a wider variety of relative angles. The majority of regions in

the nightside show angles of less than  $30^{\circ}$ . Despite our use of only measurements with intermediate to minimum eigenvalue ratios greater than 2, it is worth repeating here the caveat that directions determined by MVA for regions that are nearly linearly polarized (such as the MPR and tail regions) are unlikely to be accurate [Knetter *et al.*, 2003].

#### 3.1.5. Frequencies

[22] In order to study the frequency domain of the oscillations, we use wavelet analysis. Wavelet analysis is similar to the technique of the windowed Fourier transform in that it can transform a signal in the time domain into a time-resolved signal in the frequency domain. This allows both techniques to resolve signals in the frequency domain that are nonstationary (i.e., time varying). Wavelet analysis has the further advantage that the scalability of the wavelet basis functions allows higher time resolution at the higher frequencies of the frequency domain where it is needed and lower time resolution at the lower frequencies. Torrence and Compo [1998] provide a clear introduction to wavelet analysis and its application to geophysical signals. Tarasov *et al.* [1998] give an example of its application to oscillations upstream of the Martian bow shock.

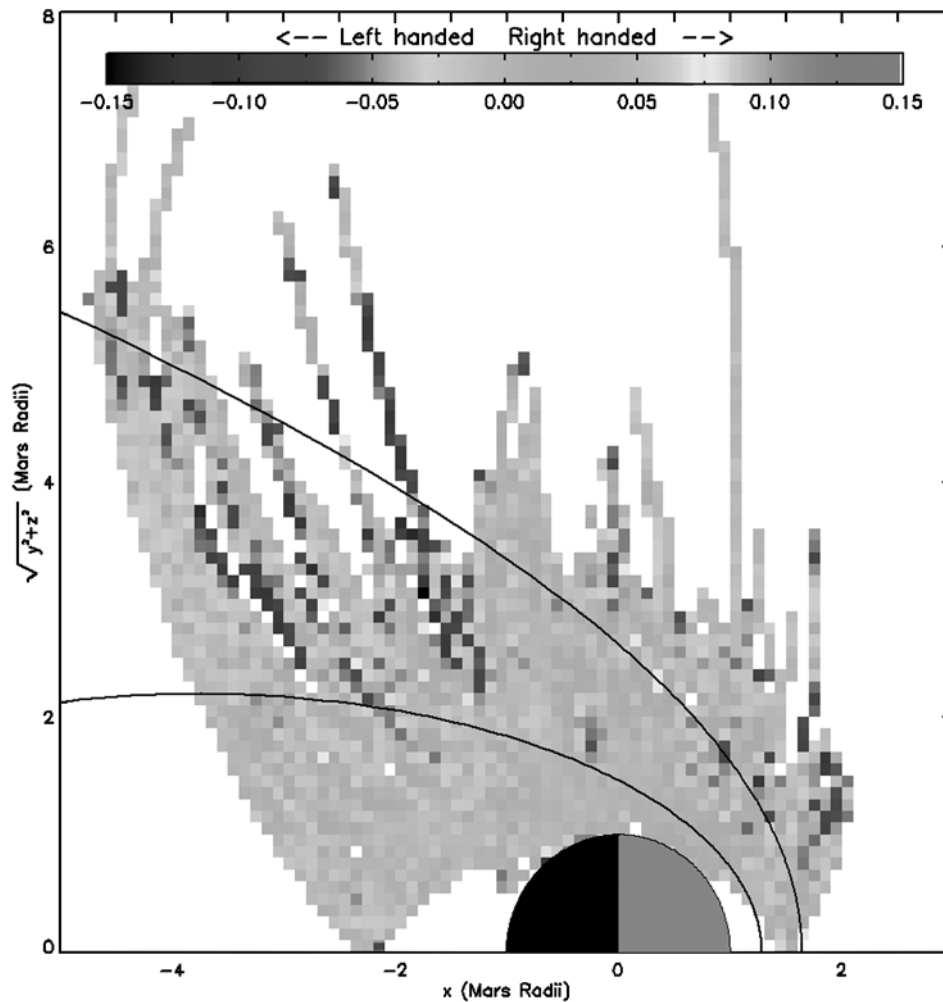


**Figure 2.** Map in SS coordinates for the sense of polarization of the oscillations about the mean field. Regions that had, on average, more left-hand polarized oscillations are shown in blue, and regions that had, on average, more right-hand polarized oscillations are shown in red. See color version of this figure at back of this issue.

[23] In our analysis we use the Morlet wavelet with a wave number of 6 because its shape gives good time localization [Torrence and Compo, 1998]. We also use a high-pass filter to reduce the spectral power due to fluctuations with frequencies less than  $\sim 0.005$  Hz. Apparent fluctuations at such frequencies could easily be created by the spacecraft passing through regions of differing plasma conditions since the spacecraft typically has a velocity  $> 5$  km/s. (For an example of a typical result, see Figure 6 and section 3.2.) Figure 5 shows a map in SS coordinates of the frequency of  $|B|$  showing the most power ( $f_o$ ) as a fraction of the local proton gyrofrequency ( $f_{H^+}$ ). In other words, we took a trace of the peak frequency for each of the 689 inbound and outbound passes that we performed wavelet analyses on and combined them to produce Figure 5. Several notable features are obvious. Within the dayside magnetosheath, the principal frequencies are significantly lower than  $f_{H^+}$  (usually between a factor of 3 and a factor of 10 lower). The nightside magnetosheath and terminator regions show more variability with the principal frequency often getting within a factor of 2 of  $f_{H^+}$ . On rare

occasions the principal frequency exceeds the proton gyrofrequency. In the MPR and the lower tail regions the principal frequencies are the lowest, usually at least an order of magnitude lower than  $f_{H^+}$ .

### 3.2. Case Studies

[24] The statistical results presented in section 3.1 give a good overview of the oscillations we are studying. However, a great deal of variety exists within the wave parameters for each individual orbit. By studying individual orbits' data in detail, we gain further insight into the general picture provided by the statistical results. We present in this subsection two case studies chosen for their ability to illustrate both the diversity of results obtained and several features commonly observed. Figure 6 shows the results of a wavelet analysis for part of the orbit on day 296 (October 23) of 1997. Figure 6a shows the decimal day and altitude versus the magnitude of the magnetic field. Two dotted vertical lines indicate the interval analyzed by wavelet analysis. Figure 6b shows that same interval on a map in SS coordinates. Figure 6c shows the wavelet power

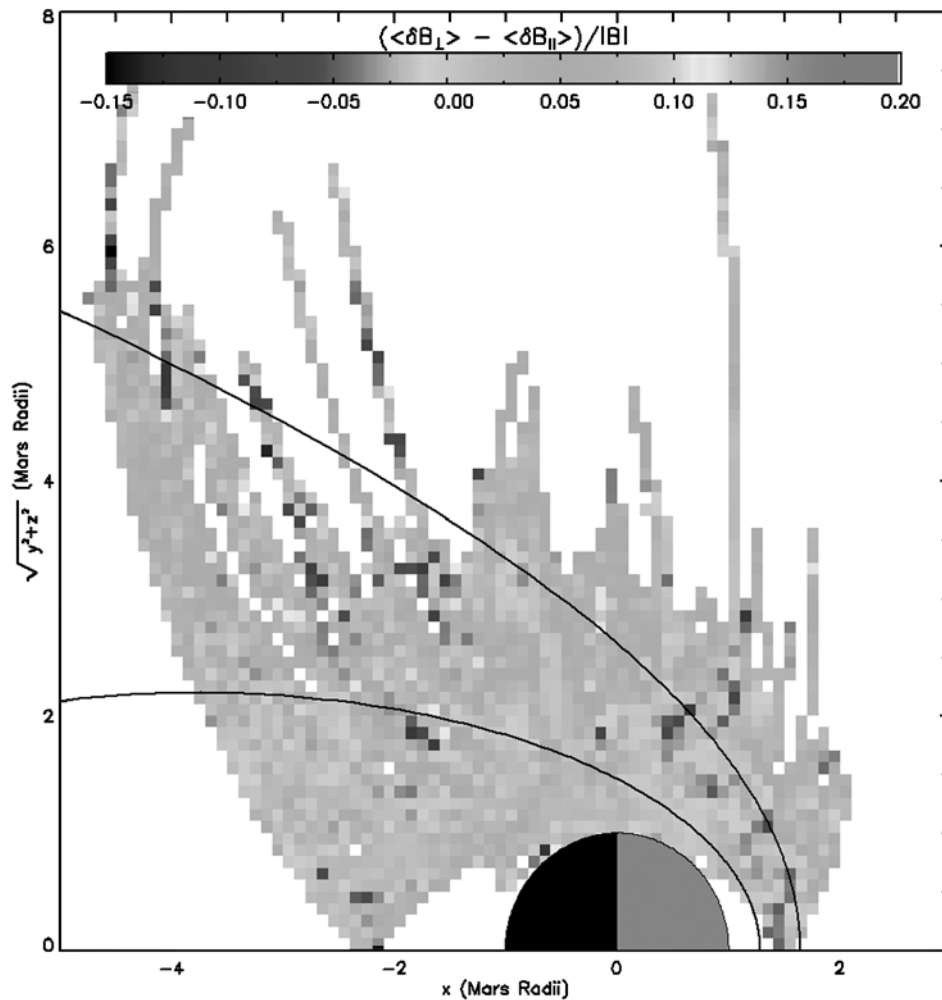


**Figure 3.** Map in SS coordinates of the differences between the average amplitude of oscillations perpendicular to the mean field and the average amplitude of oscillations parallel to the mean field. These differences are normalized by the magnitude of the magnetic field. See color version of this figure at back of this issue.

spectrum for that interval. The color scale indicates the log of wavelet power, and the higher-frequency dashed line indicates the local proton gyrofrequency, whereas the lower-frequency line indicates the local oxygen gyrofrequency. Figure 6d shows the global wavelet power spectrum (the time-integrated version of the plot in Figure 6c). The dashed line indicates the proton gyrofrequency, whereas the dotted line indicates the oxygen gyrofrequency.

[25] Two major peaks in the spectral power are apparent. One peak is at  $\sim 0.04$  Hz (about a factor of 5 times lower than the proton gyrofrequency in the magnetosheath) and starts in the MPR and continues through the magnetosheath, though it does not appear to extend upstream of the shock. Interestingly, however, this frequency is the same as the local upstream gyrofrequency, which indicates the possibility of waves being convected through the shock from upstream. The other main spectral peak is at  $\sim 0.01$  Hz, near the local oxygen gyrofrequency in the magnetosheath. This feature is relatively broad for several periods, though it appears to be artificially broadened at the edges by numerical effects. This feature matches the local oxygen gyrofrequency very well in

the region leading up to the shock and passing through it (decimal day 296.433–296.440). Spectral power at frequencies higher than the local proton gyrofrequency is apparent throughout the magnetosheath but drops off rapidly in the MPR. Spectral power upstream of the shock is considerably lower across all frequency bands (apart from edge effects). All features remarked on here are well above the 95% significance level [Torrence and Compo, 1998].

[26] Figure 7 shows the first orbit of day 31 (January 31) of 1998, which provides an additional example and includes data from the nightside magnetosheath and tail regions. In the nightside magnetosheath and far tail regions (decimal day 31.260–31.355) the frequency of highest spectral power is near 0.04 Hz, though spectral power is apparent across a wide band of frequencies (0.2–0.004 Hz) for these regions. This peak frequency is generally lower than the proton gyrofrequency by less than a factor of 2 and is especially apparent in the global wavelet power spectrum. In the near tail (decimal day 31.360–31.405) the 0.04 Hz peak largely disappears, and spectral power near the local oxygen gyrofrequency ( $\sim 0.005$  Hz) is noticeable. As in the previous example,

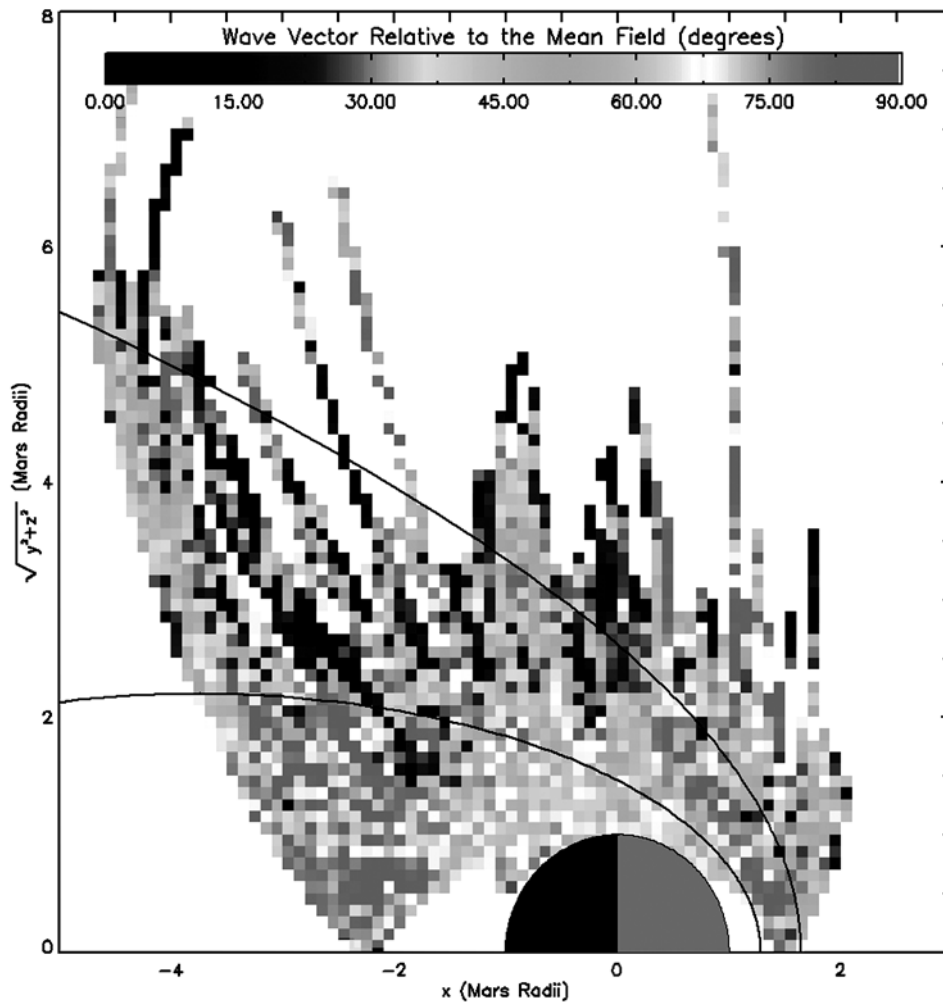


**Figure 4.** Map in SS coordinates showing the average direction of propagation (or wave vector) for the dominant wave mode for the region. See color version of this figure at back of this issue.

spectral power above the proton gyrofrequency diminished as the spacecraft approached the planet.

[27] Similar analyses have been carried out for 689 inbound and outbound passes which cover the full range of regions sampled by MGS. A website has been created (<http://spacibm.rice.edu/~espley/wavelets.htm>) which contains plots of the intervals analyzed, global wavelet spectra, and wavelet power spectra. Readers are encouraged to consult this catalog to see further examples and to study specific regions, orbits, or features.

#### 4. Discussion and Conclusions

[28] The foregoing observations create a general picture which can be summarized as follows. In the dayside magnetosheath we find somewhat elliptical, compressional oscillations (with mixed senses of polarization) which have wave vectors that are at large angles ( $>60^\circ$ ) relative to the mean field and which have dominant frequencies significantly below the proton gyrofrequency. In the nightside magnetosheath the character of the oscillations is significantly more varied, but most generally, the magnetic perturbations are left-hand elliptically polarized, transverse oscillations, which

have wave vectors with smaller angles ( $<30^\circ$ ) relative to the mean field and which have frequencies that often are closer to the proton gyrofrequency. Below the MPB and in the tail region the oscillations are ULF (more than a factor of 10 lower than the proton gyrofrequency) linearly polarized waves that are neither entirely compressional nor entirely transverse and generally propagate at large angles relative to the mean field. A full discussion and interpretation of these results from the viewpoint of theory is beyond this work. Here we present an abbreviated discussion in order to make some generalizations and to point the way for future work.

[29] Broadly speaking, two different theoretical frameworks have been used to describe low-frequency waves: either magnetohydrodynamic theories (MHD) that treat the plasma as a fluid or plasma kinetic theories based on the Vlasov equation. Fluid-based theories yield three well-known wave modes often known as the fast, intermediate, and slow modes in reference to their relative phase speeds. This fluid description, although conceptually simpler and more widely familiar, has been shown to be unlikely to be accurate for high  $\beta$  plasmas (where  $\beta$  is the ratio of particle pressure to magnetic pressure) such as planetary and cometary magnetosheaths. Several reviews [e.g., Gary, 1991,

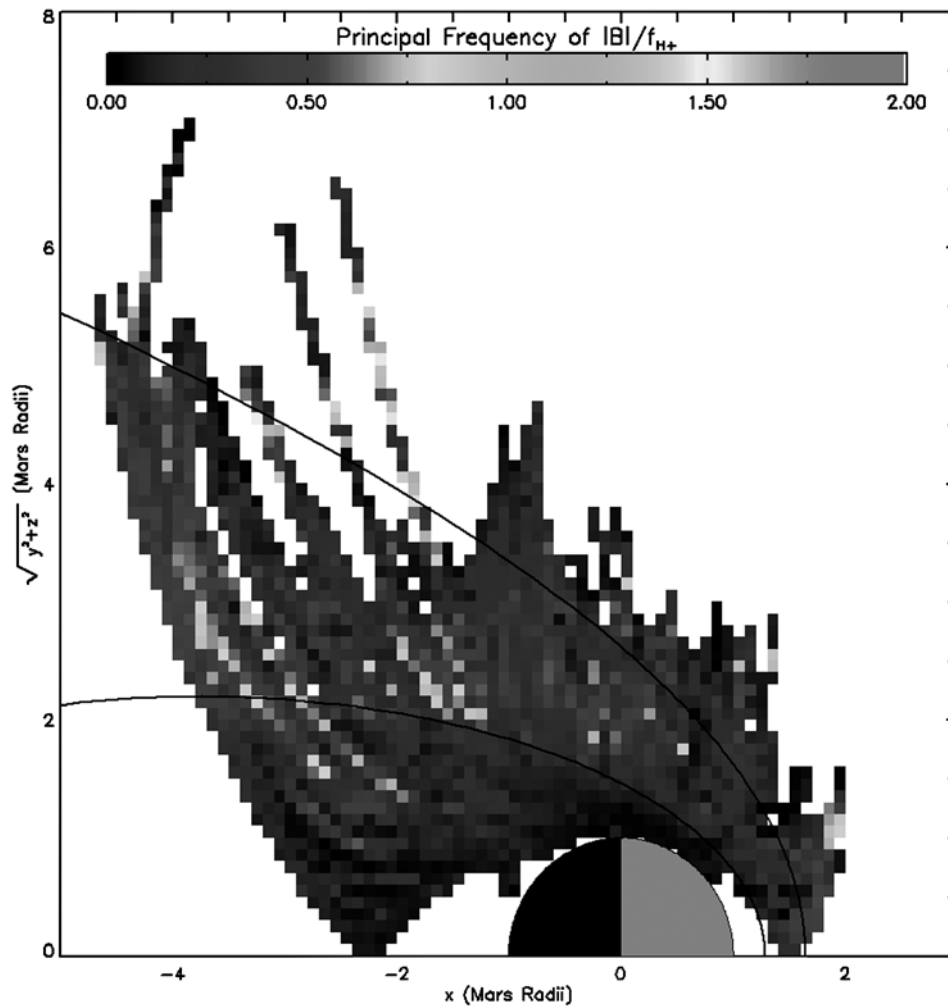


**Figure 5.** Map in SS coordinates showing the principal frequency of a region (see text for details) normalized by the local proton gyrofrequency. See color version of this figure at back of this issue.

1993; Krauss-Varban *et al.*, 1994; Schwartz *et al.*, 1996] give an overview of recent work on the subject. The simplest kinetic-based theories assume homogeneous isotropic plasma distributions and also yield three wave modes, though these modes do not correspond directly to the three MHD modes. More complicated kinetic descriptions include plasma temperature anisotropies and non-Maxwellian distribution functions (such as beams of plasma streaming past each other). Each of these complications produces changes in the possible wave modes.

[30] Gary [1992] and Gary *et al.* [1993], using kinetic theory, found that several low-frequency plasma instabilities grow for anisotropic proton-electron plasmas. In particular, when the plasma temperature perpendicular to the background field ( $T_{\perp}$ ) is greater than the plasma pressure parallel to the field ( $T_{\parallel}$ ), then two main modes develop: the mirror instability and the proton cyclotron anisotropy instability. These two instabilities grow in competition with each other whenever their anisotropy conditions are met, with the proton cyclotron instability growing faster than the mirror mode for a homogeneous plasma of  $\beta < 6$  (as is expected in the Martian magnetosheath). However, the addition of a relatively small density of heavier ions causes

the growth rate of the proton cyclotron instability to be significantly decreased and thereby allows the mirror instability to become the dominant mode in an anisotropic plasma [Price *et al.*, 1986]. Such a situation occurs in the Martian magnetosheath since the relatively large exosphere has been calculated to extend out to magnetosheath altitudes [e.g., Chen and Cloutier, 2003].

[31] In the Earth's magnetosheath, significant proton temperature anisotropies ( $T_{\perp} > T_{\parallel}$ ) are created by field compression and plasma depletion along field lines [Crooker and Siscoe, 1977]. It is plausible that similar anisotropies develop for the Martian magnetosheath, though such a plasma depletion layer has yet to be detected at Mars. It is also plausible that other mechanisms such as pickup by the solar wind of ions of planetary origin also contribute to a temperature anisotropy. Mirror mode oscillations have their largest growth rate for wave vectors with angles of  $60^{\circ}$  relative to the background magnetic field [Krauss-Varban *et al.*, 1994; Schwartz *et al.*, 1996], have real frequencies of zero in the plasma frame (and hence very low frequencies in the frame of a relatively slow moving observer), and are more compressional than transverse. These characteristics describe the oscillations that we observe in the dayside

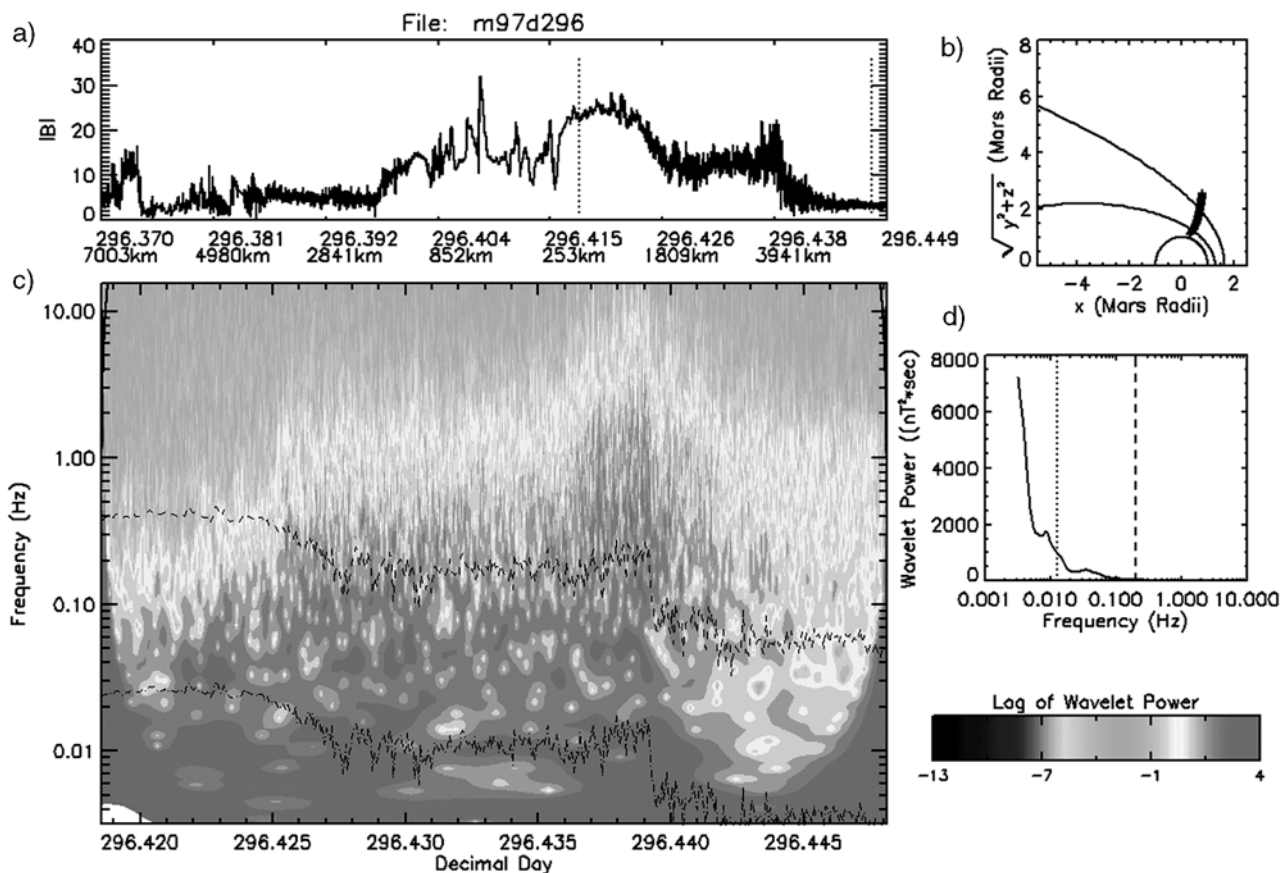


**Figure 6.** Results of a wavelet analysis for the orbit of day 296 (October 23) of 1997. (a) Decimal day and altitude versus the magnitude of the magnetic field. Two dotted vertical lines indicate the interval analyzed by wavelet analysis. (b) Same interval on a map in SS coordinates. (c) Wavelet power spectrum for that interval. (d) Global wavelet power spectrum. In Figures 6c and 6d, dashed and dotted lines indicate the local proton and oxygen gyrofrequencies, respectively. See color version of this figure at back of this issue.

magnetosheath, so we identify these oscillations as mirror mode instabilities. One potential problem with this interpretation is the fact that the oscillations are observed to be moderately elliptically polarized, and theory generally indicates that mirror modes are linearly polarized. However, *Génot et al.* [2001] have identified mirror modes in the Earth's magnetosheath that are elliptically polarized. They offer several explanations for this unexpected result, including (1) the fact that the linear theories do not account for potentially important nonlinear effects, (2) the possibility that the instabilities may couple with spatial density gradients, and (3) the possibility that several linearly polarized modes existing simultaneously may give rise to an overall elliptical polarization. Other identifications of mirror modes have been made within the Earth's magnetosheath [e.g., *Schwartz et al.*, 1996, and references therein], near the MPB of comets [*Mazelle et al.*, 1991; *Glassmeier et al.*, 1993], and near the MPB of Mars [*Bertucci et al.*, 2003b; *Bertucci*, 2003]. An additional important characteristic of mirror modes is the anticorrelation between the magnetic field strength and the plasma density. Such a characteristic could be studied by use of both the MAG and the ER data from MGS, and we leave such a study for future work.

[32] Besides describing instabilities due to plasma anisotropies, kinetic theories also give results for fluctuations due to non-Maxwellian plasma distributions (e.g., beams of plasma streaming past each other or interacting with cores or rings of different plasma populations). *Gary* [1991, 1993] gives a good summary of results from kinetic theory for various configurations of interacting plasmas. He finds that for an ion core drifting relative to a less dense ion beam, several low-frequency modes are unstable: the ion/ion right-hand resonant instability, the ion/ion left-hand resonant instability, and the ion/ion nonresonant instability. All three of these instabilities have their largest growth rates for propagation parallel to the background field, but the nonresonant instability only has significant growth when the relative drift speed between the components is significantly higher than the Alfvén speed. This is not expected to be the case downstream of the Martian shock, so we consider only the resonant instabilities. Gary finds that for a tenuous beam (such as newly formed pickup ions as seen from the frame of the solar wind) the right-hand resonant instability dominates for most  $\alpha$ , where  $\alpha$  is the angle between the solar wind velocity and the background field. However, for large  $\alpha$  ( $<75^\circ$ ) the left-hand mode dominates. Furthermore, the senses of polarization just described are in the plasma frame.

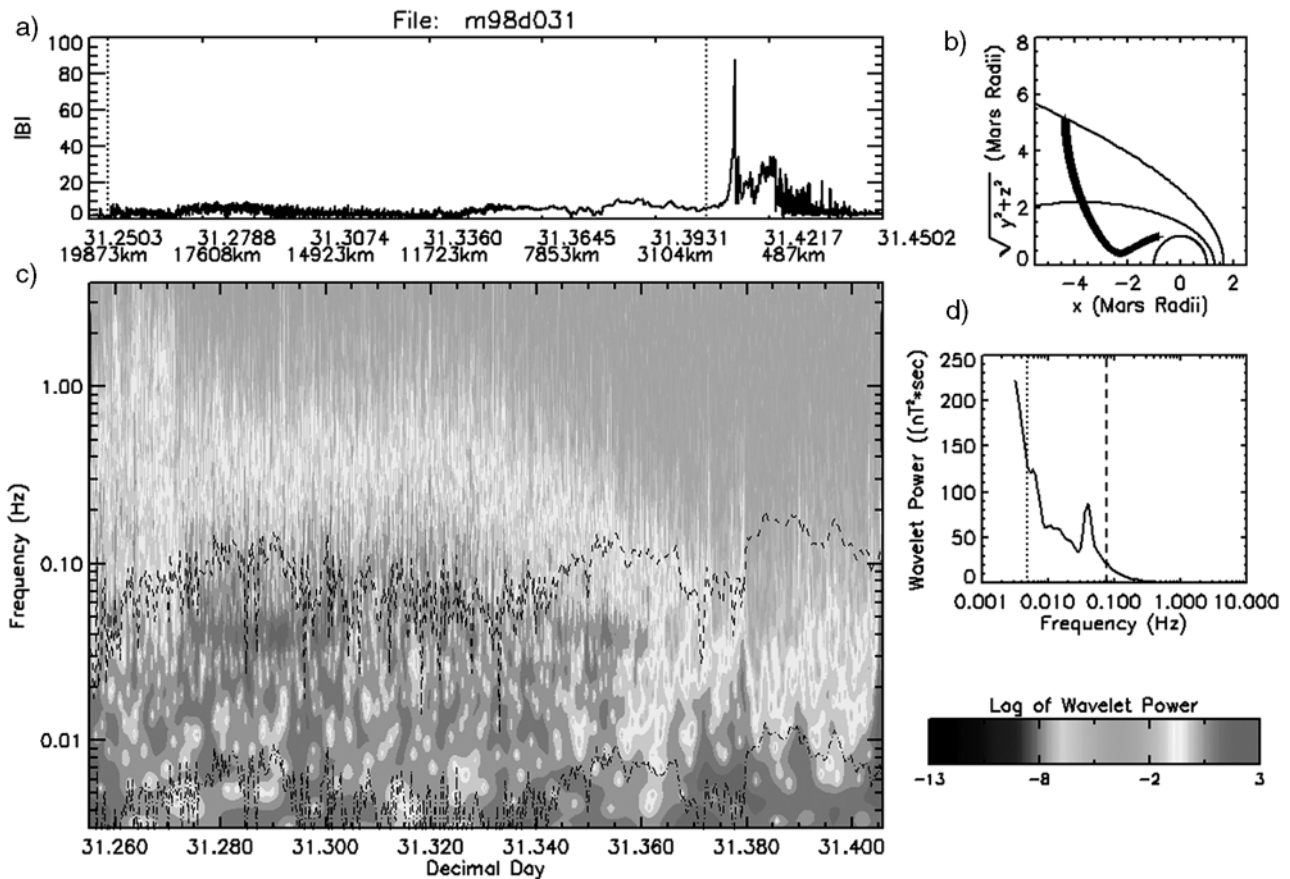


**Figure 7.** The results of a wavelet analysis for the orbit of day 31 (January 31) of 1998 in the same format as Figure 6. See color version of this figure at back of this issue.

The Doppler shift from the plasma frame to the spacecraft frame can cause the observed senses of polarization to reverse [e.g., Thorne and Tsurutani, 1987], thus making it difficult to identify specific wave modes solely on the basis of their observed senses of polarization.

[33] In contrast to their opposite senses of polarization these modes share the characteristics that they have their largest growth rates when propagating along the background field and are more transverse than compressional. Additionally, in the frame of the plasma their frequencies are typically within a factor of 2 to a factor of 10 lower than the proton gyrofrequency [e.g., Gary, 1993]. In the frame of the spacecraft these frequencies are shifted to near the proton gyrofrequency for parallel-propagating waves and to within a factor of 2 or 3 for waves with moderately oblique propagation angles [Tsurutani and Smith, 1986a]. These properties match the characteristics of many of the oscillations we observe in the nightside magnetosheath. We therefore conclude that the relatively cold, newly produced pickup ions formed from the Martian exosphere interact with the solar wind protons to produce the magnetic oscillations observed in the nightside magnetosheath. Similar identifications have been made at comets Giacobini-Zinner, Halley, and Grigg-Skjellerup (see review articles by Lee [1989], Ip and Axford [1990], and Tsurutani [1991a, 1991b]) and at Venus [Luhmann et al., 1983; Winske, 1986].

[34] Additionally, in cometary magnetosheaths, left-hand elliptically polarized oscillations near the gyrofrequency of

water group molecules have been reported [Glassmeier et al., 1987; Glassmeier and Neubauer, 1993; Neubauer et al., 1993]. Gary et al. [1993] report that kinetic modes related to cyclotron motion of heavy ions in a predominantly proton plasma are possible. Our statistical results are inconclusive with regard to the existence at Mars of oscillations near the oxygen gyrofrequency, but individual orbits do exhibit signs of such wave modes (see Figures 6 and 7). Such signals represent an observational detection of the ongoing erosion of the Martian atmosphere and its loss to space. This important topic is the subject of future work.

[35] The MPR and tail are marked by a significant decrease in magnetic field oscillatory activity. The linearly polarized, ultralow-frequency oscillations that are sometimes observed in these regions may be associated with processes occurring at the MPB, or they may be related to current systems created in the ionosphere. The fact that in these regions we observe nearly equal compressional and transverse amplitudes and the fact that the linear polarization makes determination of the wave vector direction difficult means that a definitive identification of the wave modes is problematic. It is likely that several wave modes are present in these regions, and we are observing their combined characteristics. Bertucci [2003] uses fluid theory to make an identification of fast-mode MHD waves in the MPR during some orbits. Such an interpretation is consistent with the observations we present here. More complete characterization and identification of the oscillations in this region are left to future work.

[36] We have presented observations made by MGS of the magnetic oscillations downstream of the Martian bow shock. We identify the oscillations in the dayside magnetosheath as mirror mode instabilities, whereas the oscillations in the nightside magnetosheath are associated with ion cyclotron instabilities. We note the effects of the oxygen exosphere on the instabilities and point out that such effects are signs of ongoing atmospheric loss at Mars. Finally, we identify several areas for future work and encourage readers to make use of our online catalog of results in order to identify specific orbits on which to perform further analysis.

[37] **Acknowledgments.** We are grateful for useful discussions with C. Bertucci, J. Connerney, P. Gary, C. Knez, D. Kocevski, C. Mazelle, D. Streutker, and R. Wolf. The wavelet analysis software used in this work was based on software provided by C. Torrence and G. Compo and is available at <http://paos.colorado.edu/research/wavelets/>. This work was supported by NASA grants NAG5-12728 and NGT5-156.

[38] Arthur Richmond thanks Cesar Bertucci and another reviewer for their assistance in evaluating this paper.

## References

- Acuña, M. H., et al. (1998), Magnetic field and plasma observations at Mars: Initial results from the Mars Global Surveyor mission, *Science*, *279*, 1676–1680.
- Acuña, M. H., et al. (2001), Magnetic field of Mars: Summary of results from the aerobraking and mapping orbits, *J. Geophys. Res.*, *106*, 23,403–23,417.
- Albee, A. L., R. E. Arvidson, F. Palluconi, and T. Thorpe (2001), Overview of the Mars Global Surveyor mission, *J. Geophys. Res.*, *106*, 23,291–23,316.
- Arthur, C. W., R. L. McPherron, and J. D. Means (1976), A comparative study of three techniques for using the spectral matrix in wave analysis, *Radio Sci.*, *11*, 833–845.
- Bertucci, C. (2003), Study of the interaction of the solar wind with Mars: Implications on the atmospheric escape mechanisms, Ph.D. thesis, 280 pp., Paul Sabatier Univ., Toulouse, France.
- Bertucci, C., C. Mazelle, J. A. Slavin, C. T. Russell, and M. H. Acuña (2003a), Magnetic field draping enhancement at Venus: Evidence for a magnetic pileup boundary, *Geophys. Res. Lett.*, *30*(17), 1876, doi:10.1029/2003GL017271.
- Bertucci, C., C. Mazelle, D. H. Crider, D. L. Mitchell, K. Sauer, M. H. Acuña, J. E. P. Connerney, R. P. Lin, N. F. Ness, and D. Winterhalter (2003b), MGS MAG/ER observations at the magnetic pileup boundary of Mars: Draping enhancement and low frequency waves, *Adv. Space Res.*, *33*, 1938–1944.
- Brace, L. H., R. C. Elphic, and S. A. Curtis (1983), Wave structure in the Venusian nightside ionosphere, *Geophys. Res. Lett.*, *10*, 1116–1119.
- Brain, D. A. (2002), The influence of crustal magnetic sources on the topology of the Martian magnetic environment, Ph.D. thesis, 209 pp., Univ. of Colorado, Boulder.
- Brain, D. A., F. Bagenal, M. H. Acuña, J. E. P. Connerney, D. H. Crider, C. Mazelle, D. L. Mitchell, and N. F. Ness (2002), Observations of low-frequency electromagnetic plasma waves upstream from the Martian shock, *J. Geophys. Res.*, *107*(A6), 1076, doi:10.1029/2000JA000416.
- Chen, Y., and P. A. Cloutier (2003), Martian hydrogen exosphere charge exchange with solar wind, *J. Geophys. Res.*, *108*(A10), 1381, doi:10.1029/2002JA009604.
- Cloutier, P. A., et al. (1999), Venus-like interaction of the solar wind with Mars, *Geophys. Res. Lett.*, *26*, 2685–2688.
- Crider, D. H. (1999), Evidence of electron impact ionization in the magnetic pileup boundary of Mars: Observations and modeling results, Ph.D. thesis, 109 pp., Rice Univ., Houston, Tex.
- Crooker, N. U., and G. L. Siscoe (1977), A mechanism for pressure anisotropy and mirror instability in the dayside magnetosheath, *J. Geophys. Res.*, *82*, 185–186.
- Delva, M., and E. Dubinin (1998), Upstream ULF fluctuations near Mars, *J. Geophys. Res.*, *103*, 317–326.
- Gary, S. P. (1991), Electromagnetic ion/ion instabilities and their consequences in space plasmas: A review, *Space Sci. Rev.*, *56*, 373–415.
- Gary, S. P. (1992), The mirror and ion cyclotron anisotropy instabilities, *J. Geophys. Res.*, *97*, 8519–8529.
- Gary, S. P. (1993), *Theory of Space Plasma Microinstabilities*, Cambridge Univ. Press, New York.
- Gary, S. P., S. A. Fuselier, and B. J. Anderson (1993), Ion anisotropy instabilities in the magnetosheath, *J. Geophys. Res.*, *98*, 1481–1488.
- Génot, V., S. J. Schwartz, C. Mazelle, M. Balikhin, M. Dunlop, and T. M. Bauer (2001), Kinetic study of the mirror mode, *J. Geophys. Res.*, *106*, 21,611–21,622.
- Glassmeier, K.-H., and F. M. Neubauer (1993), Low-frequency electromagnetic plasma waves at comet P/Grigg-Skjellerup: Overview and spectral characteristics, *J. Geophys. Res.*, *98*, 20,921–20,935.
- Glassmeier, K.-H., F. M. Neubauer, M. H. Acuña, and F. Mariani (1987), Low-frequency magnetic field fluctuations in comet P/Halley's magnetosheath: Giotto observations, *Astron. Astrophys.*, *187*, 65–68.
- Glassmeier, K.-H., U. Motschmann, C. Mazelle, F. M. Neubauer, K. Sauer, S. A. Fuselier, and M. H. Acuña (1993), Mirror modes and fast magnetosonic waves near the magnetic pileup boundary of comet P/Halley, *J. Geophys. Res.*, *98*, 20,955–20,964.
- Grard, R., A. Pedersen, S. Klimov, S. Savin, A. Skalsky, J. G. Totignon, and C. Kennel (1989), First measurements of plasma waves near Mars, *Nature*, *341*, 607–609.
- Grebowsky, J. M., D. H. Crider, D. S. Intriligator, R. E. Hartle, and M. H. Acuña (2003), Venus/Mars pickup ions and ionosheath wave structures, *Adv. Space Res.*, *33*, 176–181.
- Huba, J. D., and R. J. Strangeway (1997), Plasma wave phenomena at Venus, in *Venus II*, edited by S. W. Bougher, D. M. Hunten, and R. J. Phillips, pp. 95–124, Univ. of Ariz. Press, Tucson.
- Hubert, D. (1994), Nature and origin of wave modes in the dayside Earth magnetosheath, *Adv. Space Res.*, *14*, 55–64.
- Ip, W.-H., and I. Axford (1990), The plasma, in *Physics and Chemistry of Comets*, edited by W. F. Huebner, pp. 177–233, Springer-Verlag, New York.
- Jakosky, B. M., and R. J. Phillips (2001), Mars' volatile and climate history, *Nature*, *412*, 237–244.
- Knetter, T., F. M. Neubauer, T. Horbury, and A. Balogh (2003), Discontinuity observations with Cluster, *Adv. Space Res.*, *32*, 543–548.
- Krauss-Varban, D., N. Omid, and K. B. Quest (1994), Mode properties of low-frequency waves: Kinetic theory versus Hall-MHD, *J. Geophys. Res.*, *99*, 5987–6009.
- Lacombe, C., and G. Belmont (1995), Waves in the Earth's magnetosheath: Observations and interpretations, *Adv. Space Res.*, *15*, 329–340.
- Lee, M. A. (1989), Ultra-low frequency waves at comets, in *Plasma Waves and Instabilities at Comets and in Magnetospheres*, *Geophys. Monogr. Ser.*, vol. 53, edited by B. T. Tsurutani and H. Oya, pp. 13–30, AGU, Washington, D. C.
- Luhmann, J. G., M. Tatrallyay, C. T. Russell, and D. Winterhalter (1983), Magnetic field fluctuations in the Venus magnetosheath, *Geophys. Res. Lett.*, *10*, 655–658.
- Luhmann, J. G., C. T. Russell, and J. L. Phillips (1987), On the role of the quasi-parallel bow shock in ion pickup: A lesson from Venus?, *J. Geophys. Res.*, *92*, 2544–2550.
- Mazelle, C., G. Belmont, K.-H. Glassmeier, D. Le Queau, and H. Reme (1991), Ultra low frequency waves at the magnetic pile-up boundary of comet P/Halley, *Adv. Space Res.*, *11*, 73–77.
- Mazelle, C., H. Reme, F. M. Neubauer, and K.-H. Glassmeier (1995), Comparison of the main magnetic and plasma features in the environments of comets Grigg-Skjellerup and Halley, *Adv. Space Res.*, *16*, 41–45.
- McPherron, R. L., C. T. Russell, and P. J. Coleman Jr. (1972), Fluctuating magnetic fields in the magnetosphere: 2. ULF waves, *Space Sci. Rev.*, *13*, 411–454.
- Means, J. D. (1972), Use of the three-dimensional covariance matrix in analyzing the polarization properties of plane waves, *J. Geophys. Res.*, *77*, 5551–5559.
- Mitchell, D. L., R. P. Lin, H. Reme, D. H. Crider, P. A. Cloutier, J. E. P. Connerney, M. H. Acuña, and N. F. Ness (2000), Oxygen Auger electrons observed in Mars' ionosphere, *Geophys. Res. Lett.*, *27*, 1871–1874.
- Neubauer, F. M., et al. (1986), First results from the Giotto Magnetometer Experiment at comet Halley, *Nature*, *321*, 352–355.
- Neubauer, F. M., K.-H. Glassmeier, A. J. Coates, and A. D. Johnstone (1993), Low-frequency electromagnetic plasma waves at comet P/Grigg-Skjellerup: Analysis and interpretation, *J. Geophys. Res.*, *98*, 20,937–20,953.
- Omid, N., A. O'Farrell, and D. Krauss-Varban (1994), Sources of magnetosheath waves and turbulence, *Adv. Space Res.*, *14*, 45–54.
- Orlowski, D. S., G. K. Crawford, and C. T. Russell (1990), Upstream waves at Mercury, Venus, and Earth: Comparison of the properties of one Hertz wave, *Geophys. Res. Lett.*, *17*, 2293–2296.
- Orlowski, D. S., C. T. Russell, D. Krauss-Varban, and N. Omid (1994), A test of the Hall-MHD model: Application to low-frequency upstream waves at Venus, *J. Geophys. Res.*, *99*, 169–178.
- Price, C. P., D. W. Swift, and L.-C. Lee (1986), Numerical simulations of nonoscillatory mirror waves at the Earth's magnetosheath, *J. Geophys. Res.*, *91*, 101–111.

- Riedler, W., K. Schwingenschuh, D. Moehlmann, V. N. Oraevskii, E. Eroshenko, and J. Slavin (1989), Magnetic fields near Mars: First results, *Nature*, *341*, 604–607.
- Russell, C. T., J. G. Luhmann, K. Schwingenschuh, W. Riedler, and Y. Yeroshenko (1990), Upstream waves at Mars: Phobos observations, *Geophys. Res. Lett.*, *17*, 897–900.
- Russell, C. T., J. G. Luhmann, K. Schwingenschuh, W. Riedler, and Y. Yeroshenko (1992), Upstream waves at Mars, *Adv. Space Res.*, *12*, 251–254.
- Sagdeev, R. Z., V. D. Shapiro, V. I. Shevchenko, A. Zaiharov, P. Kiraly, K. Szego, A. F. Nagy, and R. J. Grard (1990), Wave activity in the neighborhood of the bow shock of Mars, *Geophys. Res. Lett.*, *17*, 893–896.
- Schwartz, S. J., D. Burgess, and J. J. Moses (1996), Low-frequency waves in the Earth's magnetosheath: Present status, *Ann. Geophys.*, *14*, 1134–1150.
- Song, P., and C. T. Russell (1999), Time series data analyses in space physics, *Space Sci. Rev.*, *87*, 387–463.
- Sonnerup, B. U. O., and L. J. Cahill Jr. (1967), Magnetopause structure and attitude from Explorer 12 observations, *J. Geophys. Res.*, *72*, 171–183.
- Strangeway, R. J., and G. K. Crawford (1995), VLF waves in the foreshock, *Adv. Space Res.*, *15*, 29–42.
- Tarasov, V., E. Dubinin, S. Perraut, A. Roux, K. Sauer, A. Skalsky, and M. Delva (1998), Wavelet application to the magnetic field turbulence in the upstream region of the Martian bow shock, *Earth Planets Space*, *50*, 699–708.
- Thorne, R. M., and B. T. Tsurutani (1987), Resonant interactions between cometary ions and low frequency electromagnetic waves, *Planet. Space Sci.*, *35*, 1501–1511.
- Torrence, C., and G. P. Compo (1998), A practical guide to wavelet analysis, *Bull. Am. Meteorol. Soc.*, *79*, 61–78.
- Trotignon, J. G., E. Dubinin, R. Grard, S. Barabash, and R. Lundin (1996), Martian planetopause as seen by the plasma wave system onboard Phobos 2, *J. Geophys. Res.*, *101*, 24,965–24,977.
- Tsurutani, B. T. (1991a), Cometary plasma waves and instabilities, in *Comets in the Post-Halley Era*, vol. 2, edited by R. L. Newburn et al., pp. 1171–1210, Kluwer Acad., Norwell, Mass.
- Tsurutani, B. T. (1991b), Comets: A laboratory for plasma waves and instabilities, in *Cometary Plasma Processes*, *Geophys. Monogr. Ser.*, vol. 61, edited by A. D. Johnstone, pp. 189–209, AGU, Washington, D. C.
- Tsurutani, B. T., and E. J. Smith (1986a), Hydromagnetic waves and instabilities associated with cometary ion pickup: ICE observations, *Geophys. Res. Lett.*, *13*, 263–266.
- Tsurutani, B. T., and E. J. Smith (1986b), Strong hydromagnetic turbulence associated with comet Giacobini-Zinner, *Geophys. Res. Lett.*, *13*, 259–262.
- Vignes, D., C. Mazelle, H. Reme, M. H. Acuña, J. E. P. Connerney, R. P. Lin, D. L. Mitchell, P. A. Cloutier, D. H. Crider, and N. F. Ness (2000), The solar wind interaction with Mars: Locations and shapes of the bow shock and magnetic pile-up boundary from the observations of the MAG/ER experiment onboard Mars Global Surveyor, *Geophys. Res. Lett.*, *27*, 49–52.
- Winske, D. (1986), Origin of large magnetosheath fluctuations in the magnetosheath of Venus, *J. Geophys. Res.*, *91*, 11,951–11,957.

---

M. H. Acuña, NASA Goddard Space Flight Center, Code 695.0, Greenbelt, MD 20701, USA. (mario.acuna@gsfc.nasa.gov)

D. A. Brain, Space Sciences Laboratory, University of California, Berkeley, CA, USA. (brain@ssl.berkeley.edu)

P. A. Cloutier and J. R. Espley, Department of Physics and Astronomy, Rice University, MS-108, Houston, TX 77005, USA. (pac@spacibm.rice.edu; espley@rice.edu)

D. H. Crider, Catholic University of America, c/o 106 Driftwood Dr., Gibsonville, NC 27249, USA. (dana.crider@gsfc.nasa.gov)

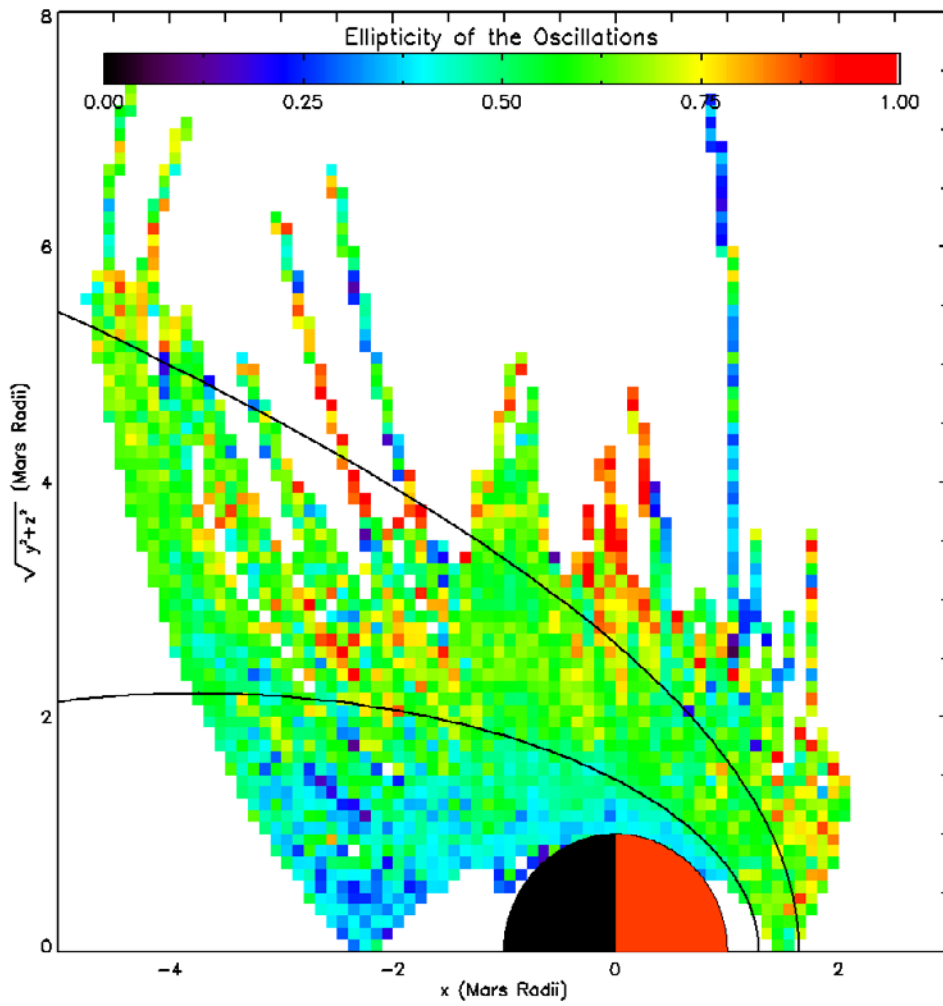


**Figure 1.** Map in Sun state (SS) coordinates of the ellipticity of the oscillations relative to the mean field.

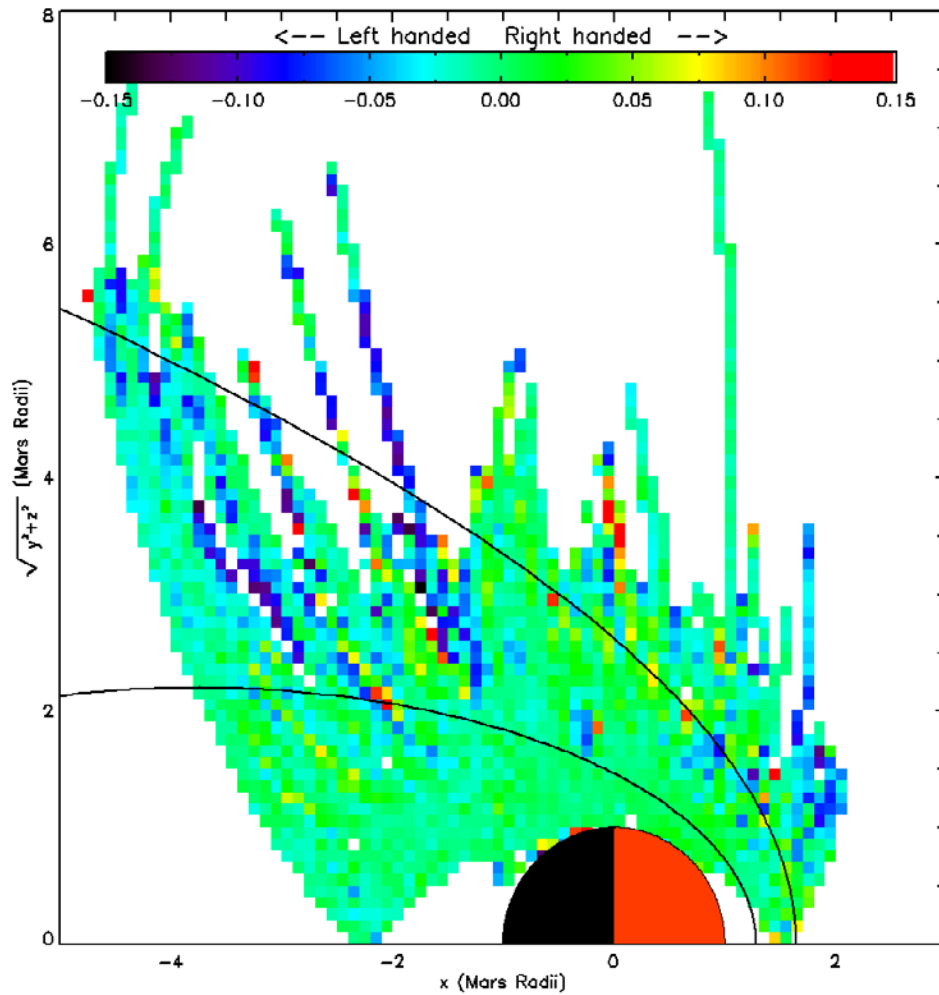


**Figure 2.** Map in SS coordinates for the sense of polarization of the oscillations about the mean field. Regions that had, on average, more left-hand polarized oscillations are shown in blue, and regions that had, on average, more right-hand polarized oscillations are shown in red.

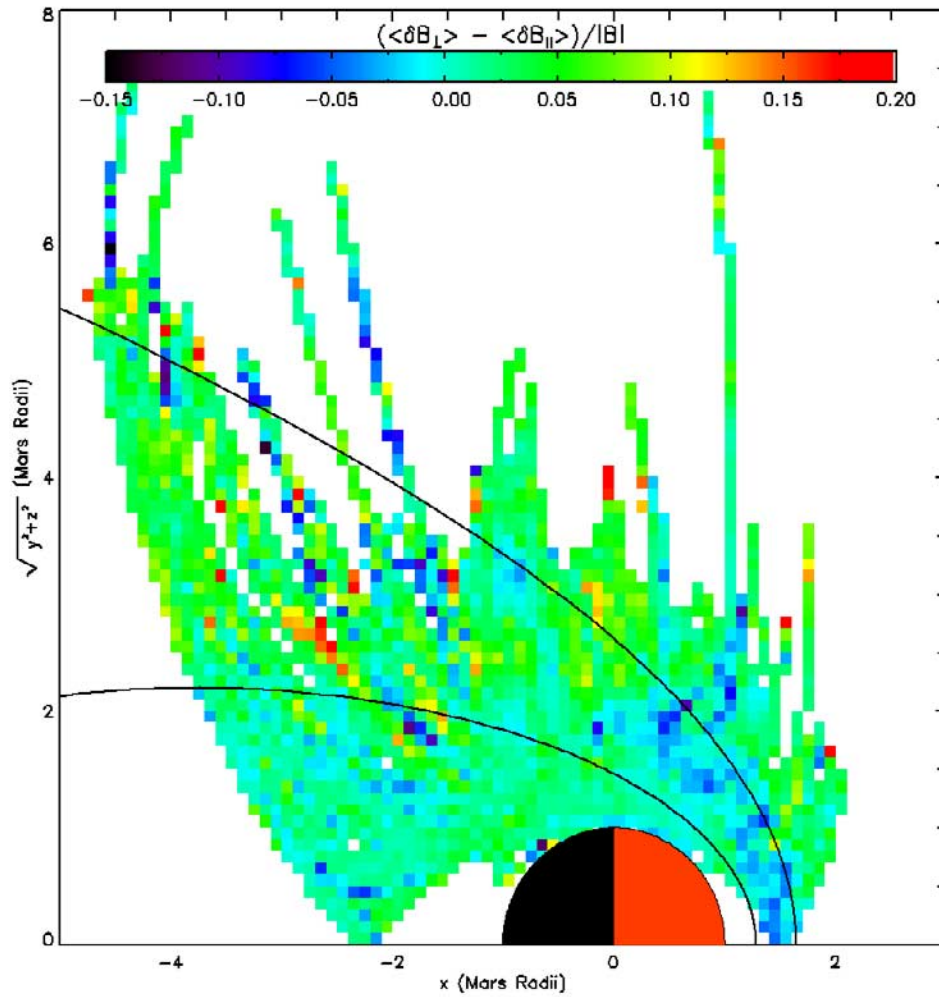


**Figure 3.** Map in SS coordinates of the differences between the average amplitude of oscillations perpendicular to the mean field and the average amplitude of oscillations parallel to the mean field. These differences are normalized by the magnitude of the magnetic field.

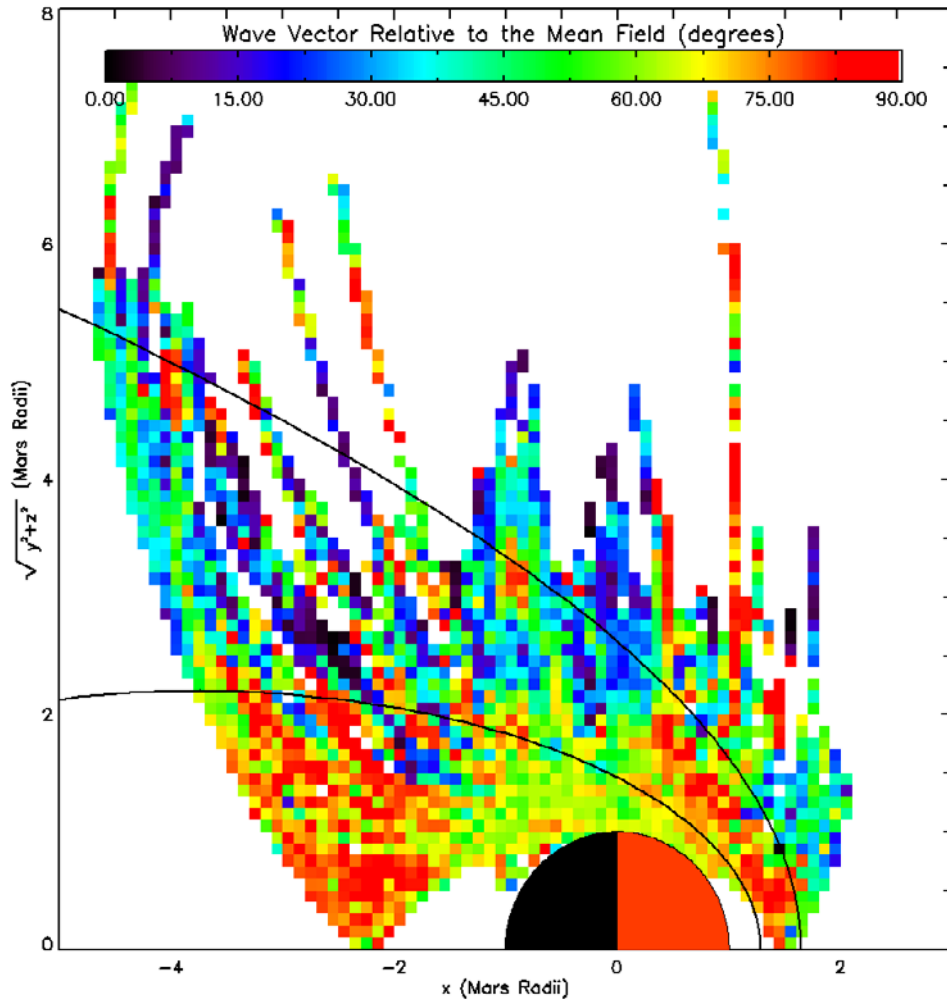


**Figure 4.** Map in SS coordinates showing the average direction of propagation (or wave vector) for the dominant wave mode for the region.

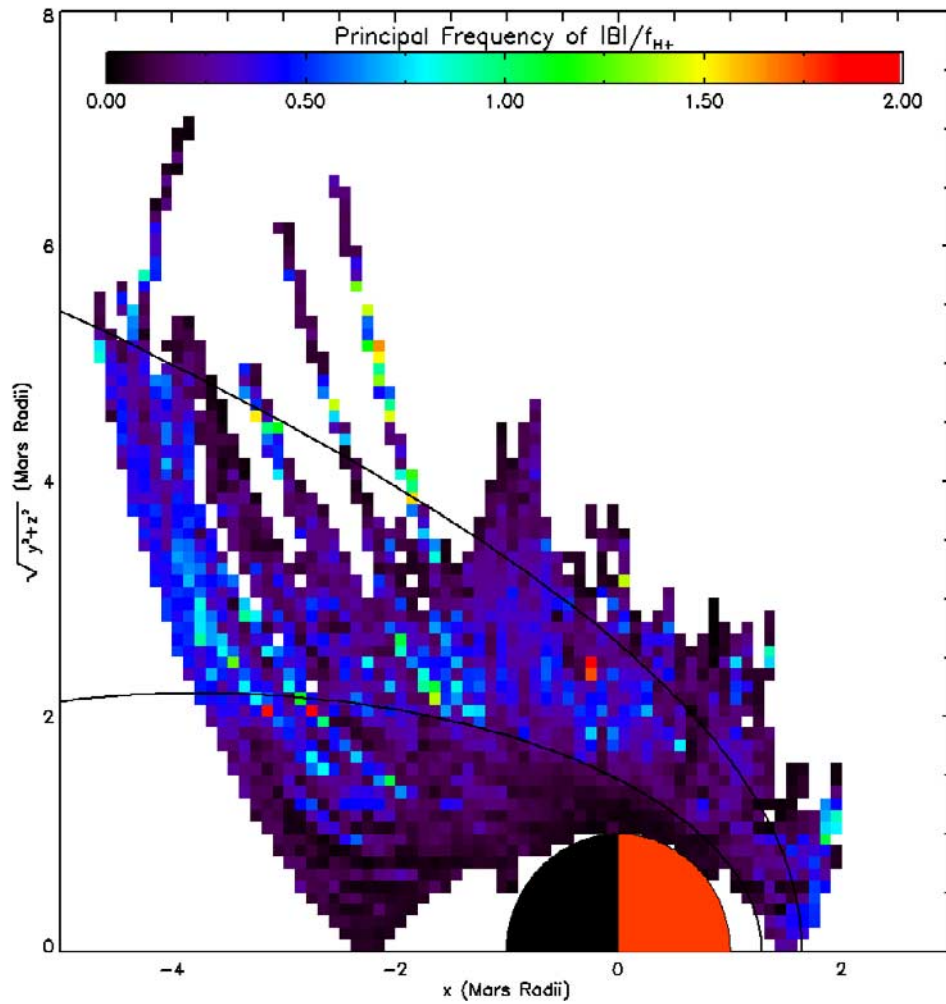


**Figure 5.** Map in SS coordinates showing the principal frequency of a region (see text for details) normalized by the local proton gyrofrequency.

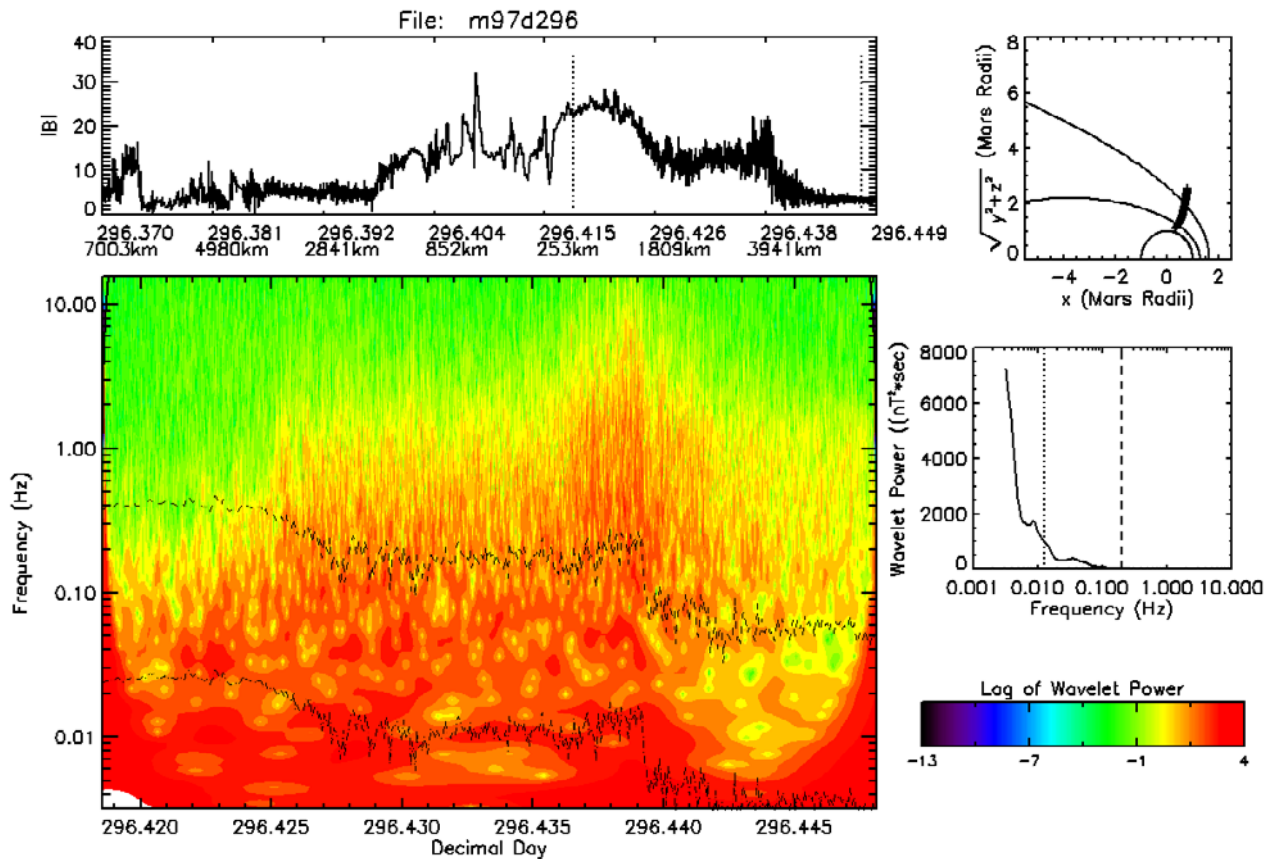


**Figure 6.** Results of a wavelet analysis for the orbit of day 296 (October 23) of 1997. (a) Decimal day and altitude versus the magnitude of the magnetic field. Two dotted vertical lines indicate the interval analyzed by wavelet analysis. (b) Same interval on a map in SS coordinates. (c) Wavelet power spectrum for that interval. (d) Global wavelet power spectrum. In Figures 6c and 6d, dashed and dotted lines indicate the local proton and oxygen gyrofrequencies, respectively.

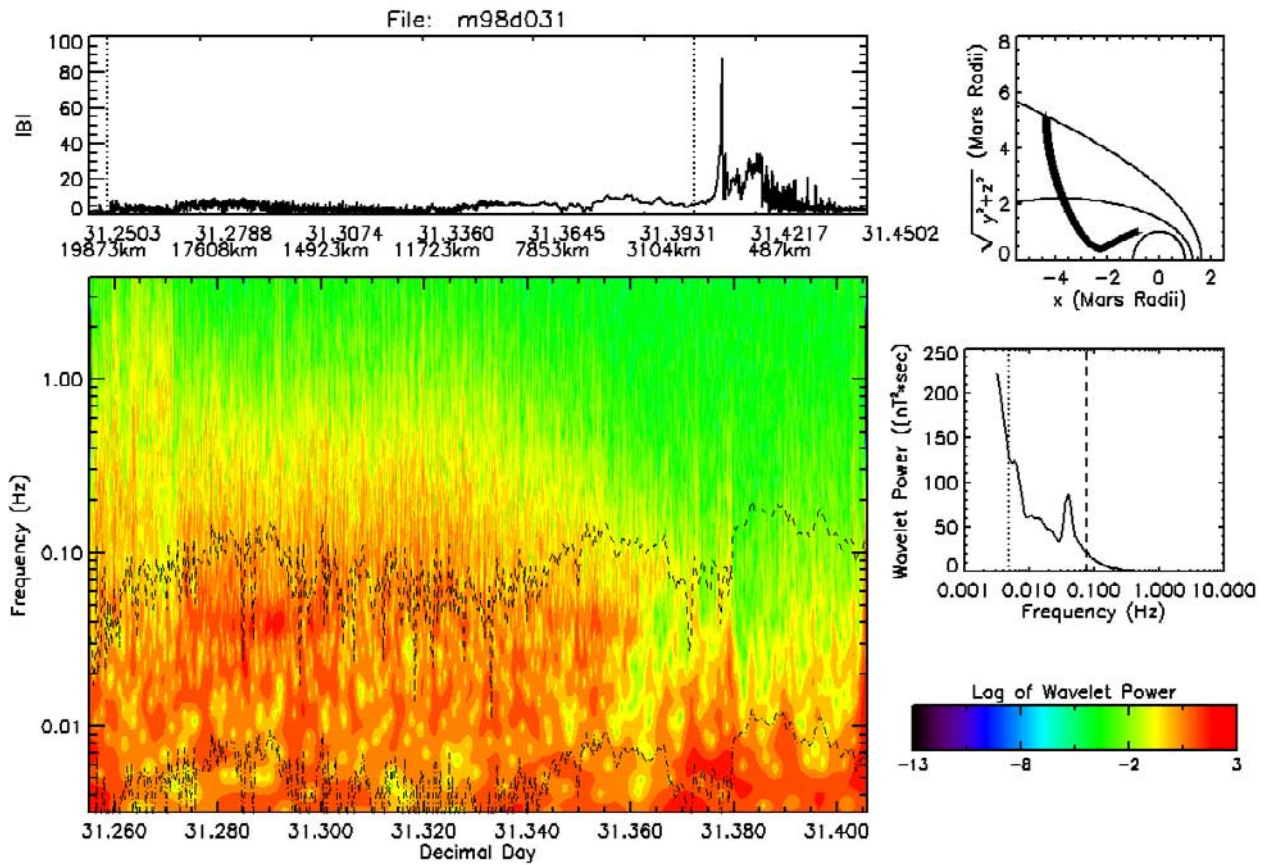


**Figure 7.** The results of a wavelet analysis for the orbit of day 31 (January 31) of 1998 in the same format as Figure 6.